Journal of Solid State Chemistry **160,** 322–331 (2001)
doi:10.1006/jssc.2001.9235, available online at http://www.idealibrary.com on IDEAL®

Three Forms of the Misfit Layered Cobaltite $[Ca_2CoO_3]\,[CoO_2]_{1.62}$. A 4D Structural Investigation

Sébastien Lambert, Henri Leligny, and Dominique Grebille

Laboratoire CRISMAT (CNRS UMR 6508), ISMRA, 6 Bd Maréchal Juin, 14050 Caen, France
E-mail: lambert@ismra.fr

Received December 18, 2000; in revised form May 1, 2001; accepted May 11, 2001

Three misfit layer compounds with the same chemical formula $Ca_3Co_{4-x}O_{9+\delta}$ were isolated in the Ca–Co–O system. They exhibit either a monoclinic or an orthorhombic symmetry. These crystals are constituted of two interpenetrating C sublattices showing incommensurate periods along the *b* axis. The structure of the three crystals can be described as an alternate stacking along [001] of distorted rock-salt-type slabs $[Ca_2CoO_3]$ and of $[CoO_2]$ layers displaying a distorted CdI_2-type structure. Relating to the symmetry and the different observed *c* periods, different sequences are found for the $[CoO_2]$ layers running along [001] within the three crystals. Two of them were determined by single X-ray diffraction using the 4D superspace formalism. A significant displacive modulation is implied, acting mainly on Ca and O atoms involved in the intersystem bonding scheme. This modulation leads to a noticeable distortion of the CoO_6 octahedra of the $[CoO_2]$ layers. Strong interactions, via Ca–O bonds, are evidenced between the two sublattices. A systematic positional disorder is observed inside the [CoO] layer. © 2001 Academic Press

Key Words: **cobalt oxide; $Ca_3Co_4O_9$; misfit; modulations; incommensurate structure.**

1. INTRODUCTION

The recent discovery of thallium and bismuth cobaltites, with a misfit layer structure (1–3), closely related to that observed in chalcogenides systems (4, 5), has opened the route to the exploration of bidimensional cobalt oxides. Recently, a new misfit cobaltite was obtained for the approximate composition $Ca_3Co_4O_9$, which was formulated $[Ca_2CoO_3]\,[CoO_2]_{1.62}$ (6). In fact, the Ca–Co–O system exhibits a complex phase diagram, since close to the latter stoichiometry $Ca_3Co_{4-x}O_{9+\delta}$ oxides were recently reported (7, 8). Their structure seems to be related to a different structural-type $Ca_2Co_2O_5$, previously described by Vidyasagar *et al.* (9).

The calcium cobalt oxides, close to the composition $Ca_3Co_4O_9$, are of great interest from a physics point of view, as shown by their thermoelectric (7, 8) and their magnetoresistance properties (6). In order to understand the origin of the physical properties of these oxides, and especially of the complex misfit cobalt oxides, an accurate determination of the atomic positions is required. To date, only one structural refinement using single-crystal diffraction data has been carried out in such misfit oxides for $[Bi_{0.87}SrO_2]_2\,[CoO_2]_{1.82}$ (10, 11). For this reason we have considered again the Ca–Co–O system, focusing our efforts on the crystal growth and structural study of these oxides.

In the present study, three different forms of the misfit layered structure, $[Ca_2CoO_3]\,[CoO_2]_{1.62}$, were synthesized as single crystals. We show that one of these composite structures with the stacking *c* parameter of 10.76 Å corresponds to the phase previously described (6), whereas the two other forms with *c* parameters of 21.52 and 32.47 Å are new polytypes. The detailed single-crystal structure determination of the two latter forms, in the 4D superspace formalism, evidences a displacive modulation, and a systematic positional disorder in the [CoO] layers of these oxides.

2. EXPERIMENTAL

2.1. Synthesis

The crystals of $[Ca_2CoO_3]\,[CoO_2]_{1.62}$ were prepared in two stages. A precursor was first synthesized, using calcium oxide CaO and the cobalt oxide Co_3O_4. The reactants were weighed according to the above formula. The mixture was pressed into the form of bars and heated at 900°C for 24 h. Second, bismuth oxide Bi_2O_3 and the melted K_2CO_3 were added in ratio Bi/Ca = 0.85 and in ratio K/Ca = 25. Cobalt oxide was also added to prevent decomposition into $Ca_3Co_2O_6$ at higher temperature. As observed, the use of Bi makes it possible to stabilize the phase. The preparation was heated up to 880°C, at 100°C/h, kept at this temperature for 100 h and then slowly cooled. Single crystals were mechanically isolated from the solidified material after dissolving the molten part in water. The samples are platelet-shaped.

0022-4596/01 $35.00

2.2. X-Ray Diffraction

A preliminary study (crystal quality and symmetry) was carried out both from Weissenberg and precession photographs, showing the composite character of the crystals. Three related phases of same chemical formula $[Ca_2CoO_3][CoO_2]_{1.62}$ established from EDS analysis were identified. No significant Bi presence could be detected from EDS analysis. They exhibit quite similar a, b_1 (first sublattice), and b_2 (second sublattice) cell parameters but different periods along [001], 10.75, approx. 2×10.75, and approx. 3×10.75 Å. Hereafter, they will be denoted phases 1, 2, and 3 respectively. Only crystals of phases 2 and 3 were found to show a sufficient quality for X-ray data collection and structure refinement. However for all the crystals of phase 3, diffuse $[001]^\star$ streaks with noteable intensity were observed in the X-ray patterns, leading to difficulties in measuring the reflection intensities. Unfortunately, all the crystals of phase 1 exhibited strong disorders and twin phenomena, preventing reliable measurement of the intensities.

The diffracted intensities for phases 2 and 3 were collected on an Enraf–Nonius CAD-4 diffractometer, using monochromatized MoK_α radiation ($\lambda = 0.71073$ Å). The cell parameters of the two subsystems were refined independently from standard techniques and the reflection intensities of the two subsystems (main reflections) were measured separately. A systematic intensity collection of the satellite reflections (first and second orders) was also performed. Corrections for Lorentz and polarization effects were applied to the data set. No significant intensity variation was observed during experiment for the three standard reflections chosen for each subsystem. Absorption corrections, based on crystal morphology and using a Gaussian integration method, were applied to the reflection intensities with the JANA98 program (12). Crystal data and experimental conditions are given in Table 1.

3. SYMMETRY

Two independent lattices are systematically observed in the diffraction pattern of the crystals studied. They are both either orthorhombic (phase 2) or monoclinic (phases 1 and 3, unique axis **b**) and C centered in all cases. The cell parameters of the two subsystems v are denoted a_v, b_v, c_v with $v = 1$ or 2. The refined cell parameters are in good agreement with those previously observed ($a_1 = 4.83$ Å, $b_1 = 4.55$ Å, $b_2 = 2.82$ Å) (4). Only phase 1 was previously referred to and was described in a monoclinic symmetry. The b_1 parameter was assumed to be related to the $[Ca_2CoO_3]$ subsystem. For the three phases, the observed $\delta = b_1/b_2$ ratio (Table 1) deviates significantly from the 8/5 or 13/8 rational values, implying the incommensurate character of the composite crystals. It has been shown that symmetry of such composite phases is better described using the four-dimensional formalism for aperiodic crystals (13). Considering the main reflections of the second subsystem as satellite reflections of M^{th} order of the $h0l$ reflections of the first subsystem (15), the diffraction vector can be written $\mathbf{s}^\star = h\mathbf{a}_1^\star + k\mathbf{b}_1^\star + l\mathbf{c}_1^\star + M\mathbf{q}_1^\star$, where $\mathbf{q}_1^\star = \mathbf{a}_2^\star + \mathbf{b}_2^\star = \mathbf{a}_1^\star + \delta\mathbf{b}_1^\star$ ($a_1 = a_2$ and $c_1 = c_2$) is the modulation wave vector associated with the first subsystem. It turns out that $\mathbf{s}^\star = H\mathbf{a}_1^\star + K\mathbf{b}_1^\star + L\mathbf{c}_1^\star + M\mathbf{q}_1^{\star ir}$ ($\mathbf{q}_1^{\star ir} = \delta\mathbf{b}_1^\star$) with $H = h + M$, $K = k$, $L = l$. For the three phases, the condition hkl: $h + k = 2n$ leads to the same Bravais condition: $HKLM$: $H + K + M = 2n$ involving $(\frac{1}{2}\,\frac{1}{2}\,0\,\frac{1}{2})$ centering in 4D space. Within this description, $HKL0$ and $H0LM$ reflections are the main reflections of the first and second subsystems respectively while the others labeled $HKLM$ stand for the satellite reflections due to the mutual influence of the two composite parts.

Only for the orthorhombic phase 2 can the superspace group be foreseen without using $HKLM$ satellite reflections. Within each subsystem, the supplementary condition $0kl : l = 2n$ is observed, implying the same space group (S.G.) $Ccmm$ for the two average structures; a centrosymmetrical S.G. is assumed. This condition and the previous Bravais condition lead to $L = 2n$ for $0KL0$ reflections and to $L = 2n$ and $M = 2n$ for $00LM$ reflections. This result suggests the global condition $0KLM : L + M = 2n$ typical of a super glide mirror (^c_s). The superspace group (S.S.G.) of the subsystem $v = 1$ is $Ccmm\,(1\delta0)s00$; the S.S.G. of the subsystem $v = 2$ is related in a simple way to the previous one, interchanging in 4D space axes 2 and 4 (14–16), leading to $Cnmm$ $(1\delta^{-1}0)$. Note that, actually, the symmetry elements of the two S.S.G. are the same but with a different setting in the respective unit cells. Otherwise the number of satellite reflections measured with $I \geq 3\sigma(I)$ (Table 1) is too small to discriminate between the two conditions $0KLM$: $L + M = 2n$ and $L = 2n$. Concerning the two monoclinic phases, two S.S.G. are possible, $C2/m$ $(1\delta0)$ and $C2/m$ $(1\delta0)s0$. The actual one can be found from the $0K0M$ reflection class but the number of these measured reflections and their intensity are too small to conclude. It should be noted that the S.S.G. $C2/m\,(1\delta0)s0$ is a subgroup of $Ccmm\,(1\delta0)s00$. A noteworthy pseudo-extinction $00l$, $l \neq 3n$ is involved in the $h0l$ diffraction pattern of phase 3.

4. REFINEMENT

The refinement was carried out for F values using the JANA98 program (12). Patterson maps, calculated without the $H0L0$ common reflections, were performed to determine a structural model for each subsystem. This model is in global agreement with the model previously proposed for each subsystem of phase 1 (4). The relative ordering of the two composite parts along the a and c axes was checked up using the only $H0L0$ common reflections. The S.S.G.

TABLE 1
Details of Data Collection

	Phase 1 (assumed from Weissenberg photographs)	Phase 2	Phase 3
Chemical formula	$[Ca_2CoO_3][CoO_2]_{1.62}$	$[Ca_2CoO_3][CoO_2]_{1.62}$	$[Ca_2CoO_3][CoO_2]_{1.62}$
Crystal size (mm)		$0.174 \times 0.132 \times 0.024$	$0.168 \times 0.252 \times 0.024$
Crystal system	Monoclinic	Orthorhombic	Monoclnic
Cell parameters in Å ($T = 294$ K)			
First subsystem	$a_1 = 4.83(2)$, $b_1 = 4.54(2)$, $c_1 = 10.76(3)$, $\beta = 98(1)^\circ$	$a_1 = 4.834(1)$, $b_1 = 4.548(1)$, $c_1 = 21.518(1)$	$a_1 = 4.836(1)$, $b_1 = 4.5462(1)$ $c_1 = 32.473(5)$, $\beta = 95.86(2)^\circ$
Second subsystem	$a_2 = 4.83(2)$, $b_2 = 2.82(1)$, $c_2 = 10.76(3)$, $\beta = 98(1)^\circ$	$a_2 = 4.834(1)$, $b_2 = 2.8200(4)$, $c_2 = 21.518(1)$	$a_2 = 4.836(1)$, $b_2 = 2.8200(4)$ $c_2 = 32.473(5)$, $\beta = 95.84(2)^\circ$
Superspace Group	$C2/m(1,\delta,0)s0$	$Ccmm(1,\delta,0)s00$	$C2/m(1,\delta,0)s0$
$\delta = b_1/b_2$	1.62	1.6191(5)	1.6191(5)
Z	2	4	6
ρ (g.cm^{-3}, μ (cm^{-1})		4.729, 13.52	4.677, 11.19
Wavelength (Å)		0.71073	0.71073
θ_{max} (°), $(\sin(\theta/\lambda)_{max}$		45, 0.995	45, 0.995
Internal consistency factor R_{int} (after absorption correction)			
Subsystem 1		4.05	7.70
Subsystem 2		5.19	6.17
Extremal transmission factors			
T_{min}		0.2355	0.2101
T_{max}		0.7207	0.7648
Number of parameters to be refined		76	168
Number of parameters actually refined		60	152
Weighting scheme		$1/\sigma F^2$	$1/\sigma F^2$
Residua			
$\Delta\rho_{min}$ (e/Å^3)		-2.34	-2.94
$\Delta\rho_{max}$ (e/Å^3)		2.58	4.94
Number of unique reflections (with $I \geq 3\sigma I$)			
$HKLM$ (The whole reflections)		738	2415
Corresponding reliability factor R/wR		0.0361/0.0340	0.0702/0.0637
$HKLM$ (K or $M = 0$)		709	2127
Corresponding reliability factor R/wR		0.0344/0.0334	0.0663/0.0620
$HKLM$ (K and $M = \pm 1$)		29	286
Corresponding reliability factor R/wR		0.2067/0.2508	0.1850/0.2269

$Ccmm(1\delta0)s00$ foreseen for phase 2 and the S.S.G. $C2/m(1\delta0)s0$ for phases 1 and 3 allowed a satisfactory structural scheme to be found that explained the $H0L0$ reflections. Some problems were encountered during the refinement of the first composite part. Fourier maps calculated from the initial model showed an anomalous spread of the electron density around the Co sites in the (**a**, **b**) plane. It can be compared with the normal electron density around the Co site within the second sublattice (Fig. 1). It was explained with a split atom model considering both a main central site and four outer sites with minor occupation rates. The refinement results suggest that this model is better than this, assuming only four offset sites. This solution was also preferred to a solution assuming a central single site for the Co atom, because it implies abnormally large values of harmonic atomic displacement parameters (ADP) (17). As verified from refinement, this spread of the electron density cannot be properly described by the introduction of a displacive modulation for the Co atom. This result is consistent with weak intensity observed for the satellite reflections and holds for phases 2 and 3. An anharmonic model for ADP was also attempted but did not lead to significant improvements. However, other models cannot be discarded owing to the disorder involved in the [CoO] layers. Beside this phenomenon, a splitting of the electron density of the oxygen atoms lying in the [CoO] layer is also observed.

A displacive modulation was assumed and refined only for the atoms not affected by the presumed static disorders. The components of the displacement vector $\mathbf{U}_v^\mu$ of the μth

atom in the subsystem μ were written as Fourier series limited to the first and second harmonics,

$$U^{\mu}_{v,i}(\bar{x}^{\mu}_{4,v}) = \sum_{n=1}^{2} A^{\mu}_{v,i,n} \sin 2\pi n \bar{x}^{\mu}_{4,v} + B^{\mu}_{v,i,n} \cos 2\pi n \bar{x}^{\mu}_{4,v}$$

$$v = 1, 2 \quad i = 1, 2, 3$$

$$\bar{x}^{\mu}_{4,v} = \mathbf{q}^{\star ir}_{v} \cdot (\mathbf{r}^{\mu}_{0,v} + \mathbf{p}_v) = \mathbf{q}^{\star ir}_{v} \cdot \mathbf{r}^{\mu}_{0,v} + t_v,$$

where $\mathbf{r}^{\mu}_{0,v}$ and $\mathbf{p}_v$ are the average position of the atom μ in the origin unit cell and a lattice vector of the subsystem v respectively. As δ is irrational, all the t_v values in the [0, 1] interval are physically significant.

The possible substitution of Ca for the Bi atom (bismuth oxide was used by synthesis process) was carefully scrutinized by systematically refining the occupation of the Ca site.

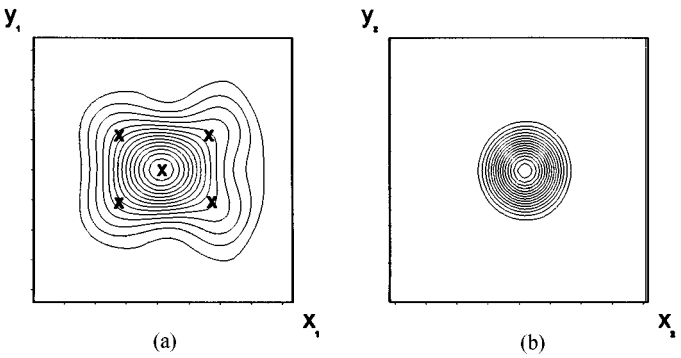

FIG. 1. Compared electron density of the Co atoms belonging to the two composite parts, (a) Co(sublattice 1) and (b) Co (sublattice 2).

The hypothesis of the noncentrosymmetric S.S.G. was also considered and tested but the refinement does not lead to any convincing improvement. The refinement parameters for phases 2 and 3 are respectively given in Table 2 and Table 3.

TABLE 2
Structural Parameters for Phase 2

Atom	Harmonic	P	x	y	z	U_{11} or U_{iso}	U_{22}	U_{33}	U_{12}	U_{13}	U_{23}
					Subsystem 1						
Ca		0.4900(5)	0.1569(1)	0	0.13723(2)	0.0064(7)	0.0098(9)	0.011(1)	0[b]	0[b]	0[b]
	$\sin(2\pi\bar{x}_4)$		0.0156(5)	0[b]	0.00044(8)						
	$\cos(2\pi\bar{x}_4)$		0[b]	0[a]	0[b]						
	$\sin(4\pi\bar{x}_4)$		0[b]	0[a]	0[b]						
	$\cos(4\pi\bar{x}_4)$		0[a]	0[b]	0.0011(1)						
Bi		0.0100(5)	0.1569(1)	0	0.13723(2)	0.017(7)					
Co(1a)		0.4824(5)	0.6584(2)	0	0.25	0.009(1)	0.018(1)	0[a]	0[b]	0[b]	0[b]
Co(1b)		0.1542(5)	0.7353(6)	0.0570(8)	0.25	0.008(1)	0.027(2)	0.0021(5)	0[a]	0[b]	0[b]
Co(1c)		0.1542(5)	0.5815(6)	0.0570(8)	0.25	0.008(1)	0.027(2)	0.0021(5)	0[a]	0[b]	0[b]
O1		1.0	0.6592(4)	0	0.1676(8)	0.0093(3)					
	$\sin(2\pi\bar{x}_4)$		0.003(1)	0[b]	0[a]						
	$\cos(2\pi\bar{x}_4)$		0[b]	0[a]	0[b]						
	$\sin(4\pi\bar{x}_4)$		0[b]	0[a]	0[b]						
	$\cos(4\pi\bar{x}_4)$		0[a]	0[b]	0[a]						
O(2a)		0.28(3)	0.066(6)	0	0.25	0.015(5)					
O(2b)		0.28(3)	0.252(6)	0	0.25	0.015(5)					
O(2c)		0.22(2)	0.159(6)	0.0672(4)	0.25	0.023(4)					
					Subsystem 2						
Co(2)		1.0	0.25	0.25	0	0.00222(7)	0.00624(9)	0.0044(1)	0[b]	0[b]	0[b]
	$\sin(2\pi\bar{x}_4)$		0[b]	0[a]	0[b]						
	$\cos(2\pi\bar{x}_4)$		0.0037(2)	0[b]	− 00207(4)						
	$\sin(4\pi\bar{x}_4)$		0[b]	− 0.0026(4)	0[b]						
	$\cos(4\pi\bar{x}_4)$		0[a]	0[b]	0[a]						
O(3)		1.0	0.5843(2)	0.25	− 0.04697(5)	0.0056(1)					
	$\sin(2\pi\bar{x}_4)$		0[b]	0[a]	0[b]						
	$\cos(2\pi\bar{x}_4)$		0.005(7)	0[b]	− 0.0012(2)						
	$\sin(4\pi\bar{x}_4)$		0[b]	0.004(2)	0[a]						
	$\cos(4\pi\bar{x}_4)$		0[a]	0[b]	0.0014(2)						

[a] Fixed because not significant within their standard deviations.
[b] Fixed by symmetry.

5. DISCUSSION

5.1. A First Description of the Misfit Structures

The three composite structures can be described as an alternation of distorted rock-salt-type slabs, formed from [CaO][CoO][CaO] layers (first subsystem) and $[CoO_2]$ layers (second subsystem), displaying a distorted CdI_2-type structure ($a_2 \simeq b_2\sqrt{3}$) stacked along [001] (Fig. 2). For phase 1, an average structural model could be suggested within the S.S.G. $C2/m$ $(1\delta 0)s0$ on the basis of the results obtained with the other phases. Concerning the $[CoO_2]$ layers, two configurations, labeled A and B, related through a (001) mirror, are observed. It appears that the different symmetries, orthorhombic and monoclinic, lead to distinct

TABLE 3
Structural Parameters for the Phase 3

Atom	Harmonic	P	x	y	z	U_{11} or U_{iso}	U_{22}	U_{33}	U_{12}	U_{13}	U_{23}
					Subsystem 1						
Ca(1)		1.0	0.5531(2)	0	0.07502(3)	0.0062(3)	0.0108(4)	0.0147(4)	0[b]	0.0019(3)	0[b]
	$\sin(2\pi\bar{x}_4)$		−0.0130(4)	0[b]	0.00027(7)						
	$\cos(2\pi\bar{x}_4)$		0[b]	−0.0019(6)	0[b]						
	$\sin(4\pi\bar{x}_4)$		0[b]	0.0033(5)	0[b]						
	$\cos(4\pi\bar{x}_4)$		−0.007(5)	0[b]	−0.0003(1)						
Ca(2)		1.0	−0.0083(1)	0	0.07502(3)	0.0069(3)	0.0103(4)	0.0158(4)	0[b]	0.0019(3)	0[b]
	$\sin(2\pi\bar{x}_4)$		−0.0146(4)	0[b]	0.00020(7)						
	$\cos(2\pi\bar{x}_4)$		0[b]	0.0042(6)	0[b]						
	$\sin(4\pi\bar{x}_4)$		0[b]	0.0011(5)	0[b]						
	$\cos(4\pi\bar{x}_4)$		0.009(5)	0[b]	0.0010(1)						
Ca(3)		1.0	0.0943(1)	0	0.045845(3)	0.0069(3)	0.0091(4)	0.0155(4)	0[b]	0.0017(3)	0[b]
	$\sin(2\pi\bar{x}_4)$		−0.0136(4)	0[b]	0.00020(7)						
	$\cos(2\pi\bar{x}_4)$		0[b]	0.0042(6)	0[b]						
	$\sin(4\pi\bar{x}_4)$		0[b]	−0.0012(5)	0[b]						
	$\cos(4\pi\bar{x}_4)$		0.0015(5)	0[b]	−0.0008(1)						
Co(1)		0.466(8)0	0	0	0	0.019(1)	0.0099(8)	0.0028(6)	0[b]	0[a]	0[b]
Co(1a)		0.150(2)	0.0761(9)	0.0592(9)	0	0.015(1)	0.022(2)	0.0050(4)	0[b]	0.0020(6)	0[b]
Co(2)		0.404(6)	0.546(1)	0	0.33330(5)	0.0084(6)	0.0175(7)	0.0050(5)	0[b]	−0.0009(2)	0[b]
Co(2a)		0.14(3)	0.472(1)	0.056(1)	0.33320(9)	0.0122(9)	0.013(1)	0.0045(5)	0[a]	−0.0016(6)	0[a]
Co(2b)		0.13(4)	0.617(1)	0.053(1)	0.33320(9)	0.0122(9)	0.013(1)	0.0045(5)	0[a]	−0.0016(6)	0[a]
O(1)		1.0	0.0345(5)	0	0.0551(1)	0.0123(6)					
	$\sin(2\pi\bar{x}_4)$		−0.002(1)	0[b]	0.0004(2)						
	$\cos(2\pi\bar{x}_4)$		0[b]	0[a]	0[b]						
	$\sin(4\pi\bar{x}_4)$		0[b]	0[a]	0[b]						
	$\cos(4\pi\bar{x}_4)$		0[a]	0[b]	0.0030(3)						
O(2)		1.0	0.5826(5)	0	0.3888(1)	0.014(1)					
	$\sin(2\pi\bar{x}_4)$		−0.003(1)	0[b]	−0.0008(2)						
	$\cos(2\pi\bar{x}_4)$		0[b]	0[a]	0[b]						
	$\sin(4\pi\bar{x}_4)$		0[b]	0.012(2)	0[b]						
	$\cos(4\pi\bar{x}_4)$		0[a]	0[b]	−0.0010(4)						
O(3)		1.0	0.5048(6)	0	0.2780(1)	0.0134(6)					
	$\sin(2\pi\bar{x}_4)$		−0.004(1)	0[b]	0.0009(3)						
	$\cos(2\pi\bar{x}_4)$		0[b]	0[a]	0[b]						
	$\sin(4\pi\bar{x}_4)$		0[b]	0[a]	0[b]						
	$\cos(4\pi\bar{x}_4)$		0.010(2)	0[b]	0.0026(3)						
O(4a)		0.129(6)	0.132(3)	0.5	0	0.0065(7)					
O(4b)		0.369(9)	0	0.429(2)	0	0.0065(7)					
O(5a)		0.283(5)	0.967(1)	0	0.3327(2)	0.029(6)					
O(5b)		0.197(5)	0.105(2)	0	0.3326(2)	0.029(6)					
					Subsystem 2						
Co(3)		0.896(2)	−0.47772(6)	0.25	0.16660(1)	0.0008(1)	0.0050(1)	0.0078(1)	0[b]	0.0008(1)	0[b]
	$\sin(2\pi\bar{x}_4)$		0[b]	0.0056(8)	0[b]						
	$\cos(2\pi\bar{x}_4)$		−0.0032(2)	0[b]	0.00144(3)						
	$\sin(4\pi\bar{x}_4)$		0[b]	−0.0008(5)	0[b]						
	$\cos(4\pi\bar{x}_4)$		0.0005(2)	0[b]	0[a]						

TABLE 3—*Continued*

Atom	Harmonic	P	x	y	z	U_{11} or U_{iso}	U_{22}	U_{33}	U_{12}	U_{13}	U_{23}
Co(4)		0.864(2)	− 0.25	0.25	0.5	0.0012(1)	0.0063(2)	0.0060(2)	0[b]	0.0013(2)	0[b]
	$\sin(2\pi\bar{x}_4)$		0[b]	0[b]	0[b]						
	$\cos(2\pi\bar{x}_4)$		− 0.0052(2)	0[b]	− 0.00144(5)						
	$\sin(4\pi\bar{x}_4)$		0[b]	− 0.0015(8)	0[b]						
	$\cos(4\pi\bar{x}_4)$		0[b]	0[b]	0[b]						
O(6)		1.0	0.1054(3)	0.25	0.53116(6)	0.0098(3)					
	$\sin(2\pi\bar{x}_4)$		0[b]	− 0.017(2)	0[b]						
	$\cos(2\pi\bar{x}_4)$		− 0.005(1)	0[b]	− 0.0015(2)						
	$\sin(4\pi\bar{x}_4)$		0[b]	− 0.010(3)	0[b]						
	$\cos(4\pi\bar{x}_4)$		0[a]	0[b]	− 0.0021(2)						
O(7)		1.0	− 0.2909(3)	0.75	0.19759(6)	0.0093(3)					
	$\sin(2\pi\bar{x}_4)$		0[b]	0[a]	0[b]						
	$\cos(2\pi\bar{x}_4)$		0.003(1)	0[b]	− 0.0021(2)						
	$\sin(4\pi\bar{x}_4)$		0[b]	0[a]	0[b]						
	$\cos(4\pi\bar{x}_4)$		0[a]	0[b]	− 0.0033(2)						
O(8)		1.0	− 0.1638(3)	0.25	0.13567(5)	0.0067(3)					
	$\sin(2\pi\bar{x}_4)$		0[b]	− 0.009(2)	0[b]						
	$\cos(2\pi\bar{x}_4)$		− 0.005(1)	0[b]	0.0006(1)						
	$\sin(4\pi\bar{x}_4)$		0[b]	− 0.027(2)	0[b]						
	$\cos(4\pi\bar{x}_4)$		− 0.002(1)	0[b]	− 0.0017(2)						

[a] Fixed because not significant within their standard deviations.
[b] Fixed by symmetry.

stacking of the $[CoO_2]$ layers, along [001], AA (phase 1), ABA (phase 2), and ABBA (phase 3) (Fig. 1). Note that correspondence between the A and B configurations is achieved through a true mirror (phase 2) or a pseudo-mirror (phase 3).

Some interesting results concerning the metric can be explained from the structural properties and the symmetry. The Ca atoms of the first subsystem have an intermediate x position between those of the neighboring oxygen atoms of the $[CoO_2]$ layers of the second subsystem. In the average structure of the different phases, all these $[CoO_2]$ layers are quite similar. According to the refined x positions, one can easily deduce a shift Δ in x position between equivalent Ca atoms at the same y position, on each side of the $[CoO_2]$ layers (Fig. 3). For an A-type $[CoO_2]$ layer (respectively B-type), this shift Δ is around $-0.314\mathbf{a}$ (respectively $+0.314\mathbf{a}$). Considering the phase 1, the AA sequence imposes a monoclinic symmetry where the β_1

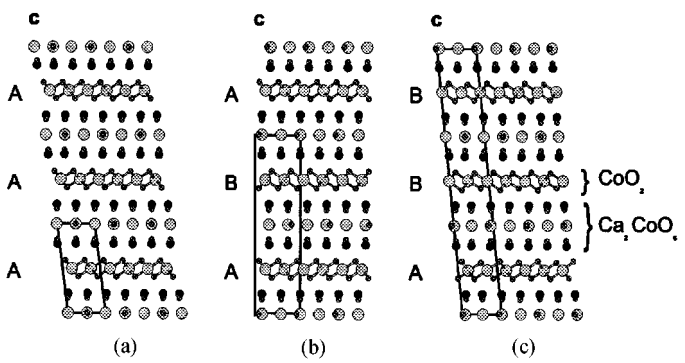

FIG. 2. Relative arrangement along **a** and **c** of the two composite subsystems ([010] projection) underlining the similar layer stacking along [001] for the three phases: (a) phase 1, (b) phase 2, and (c) phase 3.

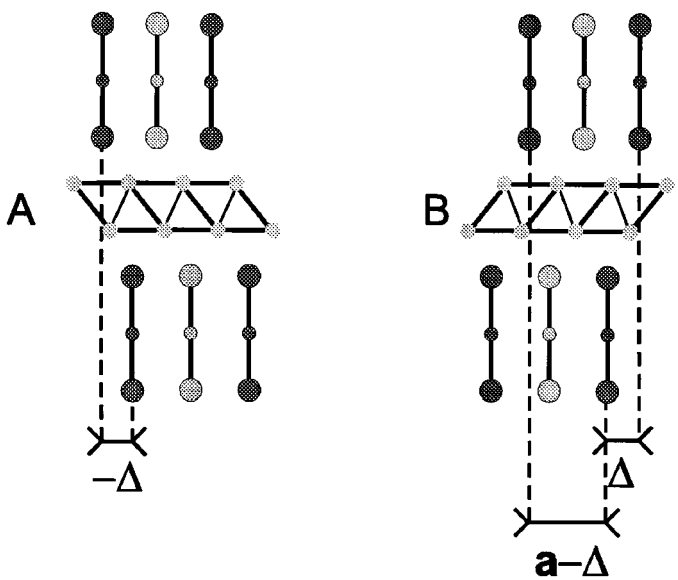

FIG. 3. Schematic representation of the relative stacking of the two neighbouring $[Ca_2CoO_3]$ layers across the $[CoO_2]$ layer.

angle is accounted from the $-\Delta$ shift ($\sin(\beta_1 - \pi/2) \approx +\Delta/c_1$). Furthermore, the existence of a local pseudo-mirror (Fig. 2a) allows the systematic twin phenomena to be explained, which replaces the AA sequence by the BB one. The ABA sequence (phase 2) is consistent with an orthorhombic symmetry, because the full shift, involved over a c period, is equal to $\Delta - \Delta = 0$. Lastly, the ABBA sequence (phase 3) leads to a monoclinic symmetry but with a β_3 angle different of β_1 ($\sin(\beta_3 - \pi/2) = (-\Delta + \Delta + (a - \Delta))/c_3$).

5.2. *The [CoO] and [CoO_2] Layers*

A main characteristic of the phases studied is indeed the existence of disorder inside the [CoO] layers of the first subsystem as shown by the refinement results. Therefore no modulations was considered for these atoms during the refinement and only the study of the oxygen environment of the central Co site can be soundly proposed.

The [CoO] layers built from regular edge-sharing CoO_6 octahedra appear as not consistent with the cell parameters $a_1 \approx 4.8$ and $b_1 \approx 4.5$ Å, which are too large. As a result, all the split oxygen sites are to be considered in the surrounding of the central Co site. The relevant Co–O distances are given in Table 4 for the phases 2 and 3. A 3+2 trigonal bipyramidal coordination for Co atoms can be considered and is coherent with layers of vertices sharing polyhedra to be built. Variants are possible involving either O(2a) or O(2b) but likely occur in different layers. Three types of interatomic distances are observed: two short apical distances (d) about 1.77 Å (Table 7), one intermediate ($d \approx 1.90$–2.15 Å), and two long ($d \approx 2.29$–2.33 Å) in the equatorial plane. Isolated CoO_6 octahedra using O(2a), O(2b), and O(2c)-type sites can also be considered with two strong apical bonds and four median bonds ($d \approx 1.95$ Å).

TABLE 4
Selected Co–O Distances *d* in [CoO] Layers Related to the Main Central Co Sites

Phase 2	*d* (Å)	Phase 3	*d* (Å)
Co(1a)–O(1)	1.773(2) ×2	Co(1)–O(1)	1.776(3) ×2
Co(1a)–O(2b)	1.96(3)	Co(1)–O(4a^{iii})	1.90(1) ×2
Co(1a)–O(2c^{vii})	1.97(2) ×2	Co(1)–O(4b)	1.95(1) ×2
Co(1a)–O(2a^{i})	1.99(3)	Co(1)–O(4a)	2.330(2) ×2
Co(1a)–O(2a^{ii})	2.313(5) ×2	Co(1)–O(4a^{iv})	2.330(2) ×2
Co(1a)–O(2b^{ii})	2.320(6) ×2		
		Co(2) – O(3)	1.786(4)
		Co(2) – O(2)	1.792(4)
		Co(2) – O(5a^{i})	2.04(1) ×2
		Co(2) – O(5b)	2.15(1) ×2
		Co(2) – O(5b^{ii})	2.289(2) ×2
		Co(2) – O(5a^{ii})	2.305(2) ×2

Note. i: $1 + x, y, z$; ii: $\frac{1}{2} + x, \frac{1}{2} + y, z$; iii: $\frac{1}{2} - x, \frac{1}{2} - y, -z$; iv: $-x, -y, -z$; vii: $\frac{1}{2} + x, -\frac{1}{2} + y, z$.

The corresponding layers should then be built from different coordination polyhedra including 3 + 2 environments likely with central Co sites and surrounding ones.

The pseudo hexagonal [CoO_2] layers are built from CoO_6 octahedra sharing half of their edges with their neighbors. For the two phases, quite similar Co–O average distances of 1.90 Å are observed inside each octahedron. Two main types of O–O distances 2.60 Å (×6) and 2.80 Å (×6) are found, the smallest O–O distances corresponding to the edge-sharing and resulting in a compressed [CoO_2] layer along [001]. The resulting strong distortion of the octahedra avoids too short Co–Co distances to be involved.

The bond valence calculation (18) applied to the Co–O bond distances leads to the following results. Inside the

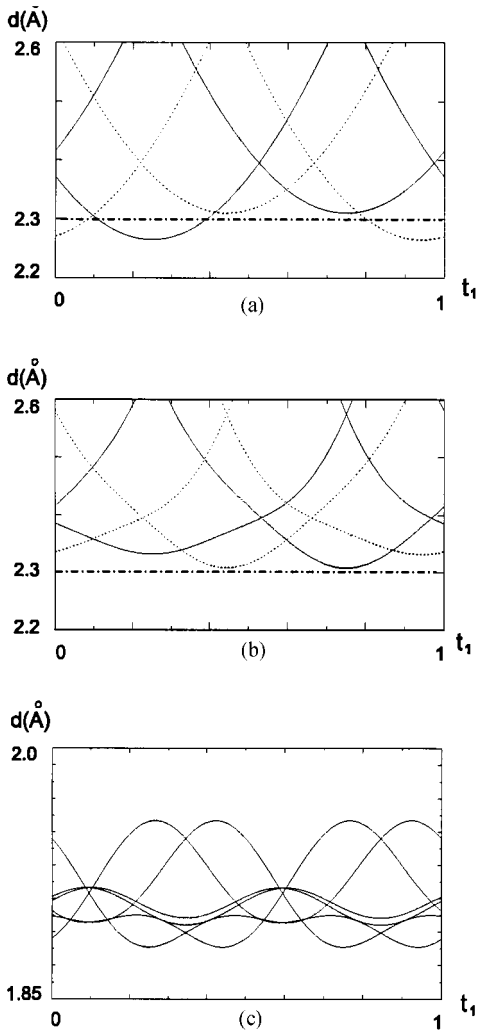

FIG. 4. Variations of the intersystem Ca–O distances (phase 2), neglecting modulation (a) and considering modulation (b) and variation of the Co–O distances in the [CoO_2] layer versus the internal phase parameter t_1. The curves drawn with solid and dotted lines refer to Ca in x, y, z and $1/2 + x$, $1/2 + y$, z positions (Figs. 3A, 3B), respectively.

TABLE 5
Minimum and Maximum Ca–O Distances *d* inside the First Subsystem

Phase 2	d_{min} (Å)	d_{max} (Å)	Phase 3	d_{min} (Å)	d_{max} (Å)
Ca–O(1^{vi})	2.352(2)	2.381(2) ×2	Ca(1)–O(1^{ii})	2.331(1)	2.403(1) ×2
Ca–O(2c)	2.420(3)	2.482(3) ×2	Ca(1)–O($4b^{iii}$)	2.434(2)	2.463(2) ×2
Ca–O(2a)	2.437(5)	2.493(5)	Ca(1)–O(1^{i})	2.437(3)	2.564(3)
Ca–O(1^{v})	2.437(3)	2.553(3)	Ca(1)–O($4a^{iii}$)	2.46(1)	2.51(1)
Ca–O(2b)	2.444(6)	2.519(6)	Ca(1)–O($4a^{vii}$)	2.47(1)	2.49(1)
Ca–O(1)	2.453(3)	2.579(3)	Ca(1)–O(1)	2.475(3)	2.625(3)
			Ca(2)–O(3^{vi})	2.325(1)	2.396(1) ×2
			Ca(2)–O(5b)	2.382(5)	2.463(5)
			Ca(2)–O(3)	2.387(3)	2.560(3)
			Ca(2)–O(5a)	2.395(5)	2.464(5)
			Ca(2)–O(3^{v})	2.468(1)	2.569(1)
			Ca(3)–O(2^{vi})	2.294(1)	2.418(1) ×2
			Ca(3)–O(5b)	2.437(5)	2.509(5)
			Ca(3)–O(2^{v})	2.438(3)	2.528(3)
			Ca(3)–O(5a)	2.452(5)	2.507(5)
			Ca(3)–O(2)	2.452(3)	2.572(3)

Note. i: $1 + x, y, z$; ii: $\frac{1}{2} + x, \frac{1}{2} + y, z$; iii: $\frac{1}{2} - x, \frac{1}{2} - y, -z$; v: $-1 + x, y, z$; vi: $-\frac{1}{2} + x, -\frac{1}{2} + y, z$; vii: $\frac{1}{2} + x, -\frac{1}{2} + y, z$.

$[CoO_2]$ layers a mixed valence state of 3.5 is obtained. Inside the [CoO] layers, the valence sum will depend on the choice of the disorder sites involved in the environment. A valence of 2.5 is calculated for the Co atoms in the bipyramidal coordination while a value of 3.5 is found in the octahedral coordination. Giving an appropriate and approximate weight to these valence states, derived from the oxygen populations, an average valence state of about 2.8, consistent with the global charge balance, is obtained. Finally, the results concerning the average valence states of Co make it possible to assume an electronic charge transfer from the [CoO] layers to the $[CoO_2]$ layers, which explains the mixed valence in this last one.

5.3. Modulation Characteristics

A small but significant displacive modulation is involved inside the two phases 2 and 3. It explains in a satisfactory way the observed intensities of the HKL $\pm$ 1 satellite reflections. The relatively high value obtained for the *R* factor (Table 1) is likely due to the weak intensity of this class of reflections. Indeed, a quite similar *R* statistic is observed for the weak main reflections. As expected, the displacive modulation acts mainly on the atoms that are involved in the intersubsystem bonding scheme. The Ca atoms (first subsystem) undergo main displacement along [100] while the oxygen atoms (second subsystem) of the $[CoO_2]$ layers move preferentially along the [010] misfit direction (Tables 2 and 3).

These displacement characteristics give rise inside phase 2 to a significant increase of the minimum Ca–O intersubsystem distances in reference to an average structure (Fig. 4). It should be also noted that noteable variations of the Co–O (Fig. 4) and O–O distances in the $[CoO_2]$ layers are involved. The resulting distortions of the CoO_6 octahedra appear rather surprising in so far as rigid body behavior could be expected for CoO_6 octahedra in a CdI_2-type layer. Furthermore a remarkable correlation between the variations of the Co–O and Ca–O distances is observed (Fig. 4). The maximum distortions of CoO_6 octahedra occur in the unit cells where the Ca–O intersubsystem distances are minimum. Concerning phase 3, the action of the modulation is less obvious. A similar behavior is observed for the minimum Ca–O intersubsystem distances related‘ to the Ca_2

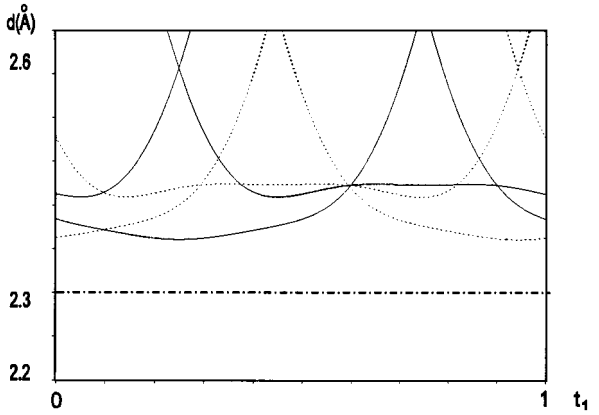

FIG. 5. Variation of the intersystem Ca(2)–O(7) distances (phase 3) versus the internal phase parameter t_1. The curves drawn with solid and dotted lines refer to Ca in x, y, z and $1/2 + x, 1/2 + y, z$ positions respectively.

TABLE 6
Compared Minimum Intersystem Ca–O Distances ($\sigma \approx 0.002$ Å) of Phase 3 within the Modulated (d) and the Average (d^*) Composite Structure

Phase 3	d_{min} (Å)	d^*_{min} (Å)
Ca(1)–O(8^{ii})	2.265	2.324
Ca(1)–O(8^{i})	2.266	2.280
Ca(2)–O(7^{vii})	2.361	2.327
Ca(2)–O(7)	2.410	2.281
Ca(3)–O(6^{vi})	2.333	2.318
Ca(3)–O(6^{ix})	2.377	2.273

Note. i: $1 + x, y, z$; ii: $\frac{1}{2} + x, \frac{1}{2} + y, z$; vi: $-\frac{1}{2} + x, -\frac{1}{2} + y, z$; viii: $\frac{1}{2} - x, \frac{1}{2} - y, 1 - z$; ix: $-x, 1 - y, 1 - z$. The intersystem Ca–O distances of phase 2 are drawn in Fig. 4 as a function of the internal phase parameter t_1.

and Ca_3 atoms (Table 6), but the smallest Ca–O distances are distributed over a t range larger than that in the orthorhombic phase (Fig. 5). In contrast for the Ca_1 atom located between two $[CoO_2]$ layers of same configuration (B), the displacive modulation shortens the minimum average Ca–O intersubsystems distances (Table 6). Otherwise, the variation amplitudes of the Co–O distances in CoO_6 octahedra are more important in phase 3 than in phase 2 (Table 7 and Fig. 4). The existence of Co vacant sites suggested by the refinement results (Table 3) could be related to this property.

The minimum and maximum Ca–O distances observed inside the first sublattice are given in Table 5. The average Ca–O distances (d) are ranged in the same rather narrow interval ($d \approx 2.35$–2.55 Å) for phases 2 and 3 (Table 5). Otherwise, within each Ca environment, Ca–O distances are significantly shorter than the others and correspond to strong bonds established along the [010] misfit direction. Table 6 shows also the existence of short Ca–O distances between the two subsystems in some unit cells. As a result, in these unit cells three strong bonds with $d \approx 2.35$ Å (two bonds along [010], the third one in (010) plane) are established, reinforcing locally the cohesion between the two composite parts. This local strong interaction between the two subsystems was also evidenced in the misfit layer compound $[Bi_{0.87}SrO_2]_2[CoO_2]_{1.82}$ (10, 11).

TABLE 7
Minimum and Maximum Co–O Distances inside the $[CoO_2]$ Layers (Second Subsystem) for Phase 3

Phase 3	d_{min} (Å)	d_{max} (Å)
Co(3)–O(8^{vi})	1.811(2)	1.992(2)
Co(3)–O(7^{vi})	1.832(2)	1.966(2)
Co(3)–O(7)	1.855(2)	1.970(2)
Co(3)–O(8)	1.880(2)	1.923(2)
Co(4)–O(6^{vi})	1.838(2)	1.997(2)
Co(4)–O(6)	1.872(2)	1.933(2)

Note. vi: $-\frac{1}{2} + x, \frac{1}{2} + y, z$. The Co–O distances of phase 2 are drawn in Fig. 4 as a function of the internal phase parameter t_1.

6. CONCLUSION

The previous study devoted to the misfit layered structure $Ca_3Co_4O_9$ proposed an ideal structural model derived from the microscopy and powder diffraction experiment (4). Such a model could here be confirmed, with the 4D structure refinement of two related phases. These two new phases prove the existence of a possible polytypism in this layered system, based on different mutual orientations of the $[CoO_2]$ layers. The different lattice symmetries, orthorhombic or monoclinic, are a direct consequence of these different stacking schemes. According to the refined structural parameters, it should be now possible to perform structure band calculations, which would help for a better understanding of physical properties and for the confirmation of a charge transfer between the two types of layers. An issue still to be studied concerns the [CoO] layer of the first subsystem which is still characterized by an important residual disorder that still prevents any definite derivation of the Co coordination. New preparations are in progress to reduce this type of disorder.

ACKNOWLEDGMENTS

The authors thank Pr. C. Michel and B. Raveau for helpful discussions, Dr. D. Pelloquin for the EDS analysis, and Mrs. J. Chardon for her technical assistance.

REFERENCES

1. Ph. Boullay, B. Domenges, M. Hervieu, D. Groult, and B. Raveau, *Chem. Mater.* **8,** 1482 (1996).
2. Ph. Boullay, R. Seshadri, F. Studer, M. Hervieu, D. Groult, and B. Raveau, *Chem. Mater.* **10,** 92 (1998).
3. M. Hervieu, Ph. Boullay, C. Michel, A. Maignan, and B. Raveau, *J. Solid State Chem.* **142,** 305 (1999).
4. E. Mackovicky and B. G. Hyde, *Struct. Bond.* **46** (1981). G. A. Wieger and A. Meerschault, *J. Alloy. Compds.* **178,** 351 (1992).
5. J. Rouxel, *C. R. Acad. Sci. Paris II* **323,** 41–57 (1996).
6. A. C. Masset, C. Michel, A. Maignan, M. Hervieu, O. Toulemonde, F. Studer, J. Hejtmanek, and B. Raveau, *Phys. Rev. B* **62,** 166–175 (2000).
7. S. Li, R. Funahashi, I. Matsubara, K. Ueno, S. Sodeoka, and H. Yamada, *J. Mater. Chem.* **9,** 1659–1660 (1999).
8. S. Li, R. Funahashi, I. Matsubara, K. Ueno, S. Sodeoka, and H. Yamada, *Chem. Mater.* **12,** 2424–2427 (2000).
9. K. Vidyasagar, J. Gopalakrishnan, and C. N. R. Rao, *Inorg. Chem.* **23,** 1206–1210 (1984).
10. H. Leligny, D. Grebille, O. Pérez, A. C. Masset, M. Hervieu, C. Michel, and B. Raveau, *C. R. Acad. Sci. Paris IIc* **2,** 409 (1999).
11. H. Leligny, D. Grebille, O. Pérez, A. C. Masset, M. Hervieu, and B. Raveau, *Acta Crystallogr. Sect. B* **56,** 173–182 (2000).

12. V. Petříček and M. Dušek, JANA98, Inst. of Phys. Acad. of Science of the Czech Republik, Prague (1998).
13. T. Janssen, A. Janner, A. Looijenga, and P. M. de Wolff, *in* "International Tables for Crystallography" (A. J. Wilson, Ed.), Vol. **C797,** Kluwer Academic, Dordrecht (1992).
14. S. van Smaalen, *in* "Incommensurate Sandwitched Layered Compounds" (A. Meerschaut, Eds.), *Trans. Tech. Pub*., pp. 173–222, Aedermannsdorf, Switzerland (1992).
15. A. Yamamoto, *Acta Crystallogr. Sect. A* **48,** 476–483 (1992).
16. A. Yamamoto, E. Takayama-Muromachi, and F. Izumi, *Physica C* **201,** 137–144 (1992).
17. K. N. Trueblood, H. B. Burgi, H. Burzlaff, J. D. Dunitz, C. M. Gramaccioli, H. H. Schulz, U. Shmueli, and S. C. Abrahams, *Acta Crystallogr. Sect. A* **52,** 770–781 (1996).
18. N. E. Brese and M. OḰeeffe, *Acta Crystallogr. Sect. B* **47,** 192–197 (1991).